IMEKO TC15 - Experimental Mechanics - Proceedings of the
11th Youth Symposium on Experimental Solid Mechanics
Brasov, ROMANIA, 2012, May 30-June 2

EFFECTIVE ELASTIC MODULI OF CLOSED-CELL ALUMINIUM FOAMS – HOMOGENIZATION METHOD

P. KOUDELKA, T. DOKTOR, J. VALACH, D. KYTÝŘ[1], O. JIROUŠEK[2]

Abstract: *During the last decades, there has been much effort on the determination of effective elastic properties of porous metals. In this paper, the overall elastic moduli of reference aluminium foam Alporas are assessed using predictive methods based on definition of compliance contribution tensor. Surface of the foam is captured using flatbed scanner and such data are subjected to image and signal processing routines in order to obtain dimensions of the sufficient representative volume element and calculation of structural characteristics for analytical homogenization. It is shown that only the Mori-Tanaka scheme gives results close to nominal values.*

Key words: *metal foam, micromechanical properties, homogenization*

1. Introduction

Metal foams are highly porous materials with cellular structure that were developed by mimicking structures identified in nature. Among other porous metals, aluminum metal foams find wide range of applications from deformation energy absorption to noise attenuation, where their lightweight character facilitates projection of highly effective constructions. During the last decades, there has been much effort to the determination of effective elastic properties of porous metals. In this paper, the overall elastic moduli of reference aluminium foam Alporas are assessed using predictive methods (i.e. non-interaction approximation, differential scheme, etc.) based on definition of compliance contribution tensor.

2. Materials and methods

As a input data, surface of the foam (Figure 1) was captured using high resolution (4800 dpi) flatbed scanner and assessed image was subjected to image manipulation (segmentation) and analysis procedures in order to obtain structural characteristics (porosity, shape factors and aspect ratios of pores) for all further calculations. To obtain dimensions of the sufficient representative volume element (RVE), spectral analysis was applied on the segmented image data for determination of the most characteristic

[1] Petr Koudelka, Tomáš Doktor, Jaroslav Valach, Daniel Kytýř, Czech Technical University in Prague, Faculty of Transportation Sciences, Department of Mechanics and Materials, Na Florenci 25, 110 00 Prague, email: {xpkoudelka, xdoktor, valach, kytyr}@fd.cvut.cz
[2] Ondřej Jiroušek, Academy of Sciences of the Czech Republic, Institute of Theoretical and Applied Mechanics, Prosecká 76, 190 00 Prague 9, email: jirousek@itam.cas.cz

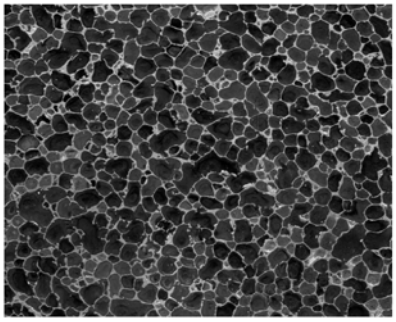

Fig. 1. *Captured surface of Alporas*

frequencies in the foam's random microstructure. Subsequently, periodicity of the microstructure is assessed and dimensions of the RVE are calculated. Homogenization procedure was utilized on the macroscopic level of foam's hierarchical structure.

2.1. Alporas

Alporas® is a light-weight cellular material with closed-cell internal structure industrially produced since 1986. Practical production is conducted by Japan company Shinko Wire Co., Ltd. that is at the European market represented by Austrian reseller Gleich, Gmbh. Its macroscopic physical and mechanical properties are almost perfectly isotropic thanks to polyhedral cell shapes with outstanding three dimensional stability, typical dimensions in interval 1 – 13 mm and average dimension 4.8 mm [9]. The foam typically exhibits 90 % porosity that can be controlled during the foaming process to certain level taking into account that polyhedral cells become spherical at porosities lower than 70 %.

3. RVE assessment

2-D image data captured using high resolution flatbed scanner were segmented to output in form of a binary image. In this image, path-lines were generated in order to define locally phase functions:

$$\phi(s) = s \cdot (x, y) \tag{1}$$

These phase functions represent the fundamentals for the spectral analysis to assess periodic character of the structure and dimensions of RVE [2]. In this paper, phase functions were generated and evaluated for every row and line in the binary array of captured foam's microstructure.

There are several ways to express mathematical basis of tools used for signal processing. For the purpose of this paper, a time history random signal function $x(t)$ has its corresponding autocorrelation function expressed by:

$$R_{xx}(\tau) = \lim_{T\to\infty} \int_0^T x(t)x(t+\tau)dt \tag{2}$$

where t and τ are time variables and T is the length of the time series. The power spectrum density (PSD) function $S_{xx}(f)$ is then defined as the Fourier transform (FT) of the autocorrelation function:

$$S_{xx}(f) = \int_{-\infty}^{\infty} R_{xx}(\tau)e^{-2\pi i f \tau}dt \tag{3}$$

where f is the signal frequency and coordinate of its maximum defines the investigated most characteristic period of the signal. This method can be also applied to other fields like in this thesis the investigation of materials with random microstructure. Here, the phase function - $\phi(s)$ is not a time history random field but depends stochastically on the spatial path

variable s . Therefore, the time variables t and τ in autocorrelation function and its corresponding PSD function are replaced by the spatial coordinates s and σ [6]:

$$R_{xx}^{n}(\sigma) = \lim_{S\to\infty}\frac{1}{S}\int_{0}^{L_s}\phi(s)\phi(s+\sigma)\mathrm{d}s \quad (4)$$

$$S_{xx}^{n}(f_s) = \int_{-\infty}^{\infty} R_{xx}^{n}(\sigma)e^{-2\pi i f_s \sigma}\mathrm{d}\sigma \quad (5)$$

where L_s is the one-dimensional path length and f_s is the structural frequency in ($\mathbf{m^{-1}}$), which is reciprocal of the searched structural period.

The PSD function is evaluated in order to detect large peaks (local and global extremes) that represent characteristic periods of the structure. Calculation of the PSD function for a limited signal/path length with discrete data points can be carried out by different spectral estimation procedures. In this study, the periodogram spectral estimation denoted by the following equation was used:

$$S_{xx}^{n}(f_s) = \frac{1}{L_s}|\hat{\phi}(f_s, L_s)|^2 \quad (6)$$

where $\hat{\phi}(f_s, L_s)$ is the discrete Fourier transform (DFT) of the phase function $\phi(s)$ given by:

$$\hat{\phi}(f_s, L_s) = \int_{0}^{L_s}\phi(s)e^{-2\pi i f_s s}\mathrm{d}s \quad (7)$$

Value of global maximum can be used as the period magnitude for the current path function. However, the location of this maximum varies even for different paths within the same cross-section and especially for 2-D input data, high caution has to be given to treatment of stochasticity in all the calculations. Therefore, in order to get the reliable structural period in each structural direction, an average over all path-lines within a 2-D cut is made. Furthermore, the input image is divided into several square regions overlapping each other by one half of its area. This ensures that each segment of generated path-lines is in the calculation included no more than twice. Such network of several overlapping regions facilitates proper characterization of the random structure with required level of reliability of results. Hence, the value of investigated period is averaged over the defined cuts per structural direction among each region and then over all generated regions.

4. Homogenization

4.1. Microstructural characterization

Porosity of the material was determined by weighting of the sample resulting in value of 91.4 %. Then, required microstructural information was extracted from the binary image leading to determination of the average aspect ratio of 3-D pores according to the following formula [5]:

$$\gamma^{3D} = \frac{3}{2}R \quad (8)$$

where R is the 2-D shape factor of pores denoted by the following equation:

$$R = \frac{1}{A}\sum_{i} A_i \gamma_i^{2D} \quad (9)$$

γ_i^{2D} is the aspect ratio, A_i is the area of *i*-th 2-D pore and A is the total area of the pores.

4.2. Effective elastic properties

In case of elastic properties investigated here for inhomogeneous materials, all calculations are based on fourth rank tensors leading to quantification of two isotropic material constants (elastic modulus and Poisson's ratio) [3]. Relations described in this section are valid for effective Young's modulus of a material containing isotropic mixtures of non-spherical pores and used prediction schemes are rooted in the non-interaction approximation and compliance contribution tensor defined as [10]:

$$\varepsilon_{ij} = S^0_{ijkl}\sigma_{kl} + H_{ijkl}\sigma_{kl} \tag{10}$$

where H-tensor depends on pore shapes and its elastic properties. For ellipsoidal pores, it is related to Eshelby's tensor by [10]:

$$H = \frac{V_p}{V}[C^0(I - S)]^{-1} \tag{11}$$

where

$$C^0 = (S^0)^{-1} \tag{12}$$

$$(I)_{ijkl} = \frac{1}{2}(\delta_{ik}\delta_{jl} + \delta_{il}\delta_{jk}) \tag{13}$$

Its components are expressed in terms of elliptic integrals for ellipsoidal pores and reduce to elementary functions in case of spheroidal pores. Calculation of these tensors can reduce to quantification of factors from the following relation when explicit analytic inversion is introduced [4]:

$$H = \frac{V_p}{V}\frac{1}{G_0}\sum_{k=1}^{6} h_k T^{(k)} \tag{14}$$

4.2.1 Non-interaction approximation

Here, the effective compliance tensor can be denoted as [11]:

$$S = S_0 + \sum_i H^{(i)} = S_0 + H_{NI} \tag{15}$$

where H_{NI} is in this case:

$$H_{NI} = p\left[\frac{\frac{3B_1 - B_2}{2}}{G_0}\left(\frac{1}{3}II\right) + \frac{B_2}{G_0}\left(I - \frac{1}{3}II\right)\right] \tag{16}$$

Shape factors B_1 and B_2 that are functions of aspect ratios and Poisson's ratio of the matrix material can be assessed by integration of Eq. 14 over all possible orientations resulting in:

$$B_1 = \frac{20h_1 + 9h_2 + 28h_3 - 4h_4 + 6h_5}{30}$$
$$B_2 = \frac{2h_1 + 11h_2 - 4h_3 + 8h_4 + 2h_5}{30} \tag{17}$$

(18)

where coefficients h_i are yielded by the explicit analytic inversion of the H-tensor. The effective Young's modulus is using this scheme predicted by the following relation (Eq. 19):

$$E = \frac{E_0}{1 + p\xi(\gamma, \nu_0)} \tag{19}$$

where:

$$\xi(\gamma,\nu_0)=2(1+\nu_0)\left(B_1+\frac{B_2}{2}\right) \quad (20)$$

Self consistent scheme leads to a system of two nonlinear equations for the bulk and shear moduli [12]:

4.2.2 Self-consistent scheme

$$K=K_0\left[1-p\frac{2(1+\nu)}{1-2\nu}\left(\frac{3B_1(\gamma,\nu)-B_2(\gamma,\nu)}{2}\right)\right] \quad (21)$$

$$G=G_0[1-2pB_2(\gamma,\nu)] \quad (22)$$

Using solution of a relation obtained by dividing the Eq. 21 by Eq. 22, the effective Young's modulus can be obtained from:

$$E=E_0[1-p\xi(\gamma,\nu)] \quad (23)$$

4.2.3 Differential scheme

Differential scheme is usually interpreted as an infinitesimal form of the self-consistent scheme which leads to a system of two differential equations for both the bulk and shear moduli [8]. Detailed analysis of these relations for spheroidal inclusions is given in [13] and the solution leads to the effective Young's modulus expressed as:

$$E=E_0\exp\left(-\int_0^p\frac{\xi[\gamma,\nu(\rho)]}{1-\rho}d\rho\right) \quad (24)$$

If one considers negligible variation of Poisson's ratio with porosity Eq. 24 reduces to:

$$E=E_0(1-p)^{\xi(\gamma,\nu_0)} \quad (25)$$

4.2.3. Effective-fields method

The Mori-Tanaka [1] and Levin-Kanaun [7] single equation schemes are ranked among effective fields method and appear in the following expressions for the effective Young's modulus:

$$E=\frac{E_0}{1+\frac{p\xi(\gamma,\nu_0)}{1-p}} \quad (26)$$

$$E=\frac{E_0}{1+\frac{p\xi(\gamma,\nu_0)}{1-p\frac{\xi(\gamma,\nu_0)}{\xi(1,\nu_0)}}} \quad (27)$$

5. Results

Using the methods discussed hereinbefore, mechanical properties of Alporas closed-cell aluminium foam were assessed. By analyzing scanned macrostructure of the foam, dimensions of the RVE were obtained by methods of spectral analysis:

$x=26.64$ mm
$y=29.45$ mm

Then 3-D shape factor resulting in value $\gamma^{3D}=0.674$ was calculated as input to the homogenization models. Table 1

summarizes obtained homogenized effective elastic moduli:

Results from the homogenization schemes Table 1

Scheme	$E_{effective}$ [GPa]
Non-interaction	16.22
Self-consistent	-
Differential	0.012
Mori-Tanaka	1.78
Levin-Kanaun	-

It is evident that these analytical schemes do not give appropriate results. This can be explained by the fact that basic assumptions following from Eshelby's solution of an ellipsoidal inclusion in an

It has been shown that considered analytical homogenization schemes, apart from the Mori-Tanaka scheme, are not suitable for determination of elastic properties of the reference foam which is

Voigt and Reuss bounds Table 2

Bound	Young's modulus [GPa]
Voigt	6.02
Reuss	0.0011

From the Table 1, one can see that the non-interaction scheme does not even fulfill the Voigt bound. As self-consistent and Levin-Kanaun schemes lead to zero elastic moduli for porosities lower than porosity of Alporas due to large volume fractions of pores (filled with air exhibiting zero mechanical properties), their values in the Table 1 are omitted for convenience. Although differential scheme fulfills the Reuss bound, it leads to substantial underestimation of the actual Young's modulus. Only the Mori-Tanaka scheme ends up close to the nominal value $E \sim 1.4$ GPa measured by uni-axial compressional tests of Alporas for verification of theoretical results.

6. Conclusion

homogenization methods employing finite element equivalence of porous microgeometries should be used.

Acknowledgment

The research has been supported by Grant Agency of the Czech Technical University in Prague (grant No. SGS12/205/OHK2/3T/16), research plan of the Ministry of Education, Youth and Sports MSM6840770043, Czech Science Foundation (grant No. P105/12/0824) and by RVO: 68378297.

References

1. Benveniste Y.: Mech. Res. Commun. Vol. 13 (1986), p. 193.
2. Bobzin K., Lugscheider E., Nickel R., Kashko T.: Adv. Eng. Mater. 8 (7) (2006), p. 663–669.
3. Eroshkin O., Tsukrov I.: Int. J. Solids Struct. 42 (2005) 409.
4. Kunin I.A.: Elastic Media with Microstructure, Springer Verlag,

Berlin, 1983.
5. Laraja V.J., Rus I.L., Heuer A.H.: J. Am. Ceram. Soc. 78 (1995), p. 1532.
6. Laschet, G. et al.: Materials Science and Engineering A 472 (2008), p. 214–226, 2007.
7. Levin V.M.: Soviet Physics Doklady 220 (1975), p. 1042.
8. Markov K.Z., in: K.Z. Markov, L. Preziozi (Eds.), Heterogeneous Media: Micromechanics Modeling Methods and Simulations, Birkhauser, Boston, 2000, p. 1.
9. Miyoshi, T., Itoh, M., Akiyama, S., Kitahara A.: Aluminium foam, "ALPORAS": The Production Process, Properties and Applications, Materials Research Society Symposium Proc. Vol. 521, 1998.
10. Sevostianov I., Kachanov M.J.: Mech. Phys. Solids 50 (2002), p. 253.
11. Sevostianov I., Kováčik J., Simančík F.: Materials Science and Engineering A 420 (2006), p. 87–99.
12. Zaoui A.: Journal of Engineering Mechanics 128, 8, 808-816 (2002).
13. Zimmerman R.W., Mech. Mater. 12 (1991), p. 17.